Proceedings of ASME Turbo Expo 2016: Turbomachinery Technical Conference and Exposition
GT2016
June 13-17, 2016, Seoul, South Korea

GT2016-57499

A SECOND TURBULENT REGIME WHEN A FULLY DEVELOPED AXIAL TURBULENT FLOW ENTERS A ROTATING PIPE

Ferdinand-J. Cloos
Chair of Fluid Systems
Technische Universität Darmstadt
Darmstadt, Hesse, 64289
Germany
ferdinand.cloos@fst.tu-darmstadt.de

Anna-L. Zimmermann
Peter F. Pelz*
Chair of Fluid Systems
Technische Universität Darmstadt
Darmstadt, Hesse, 64289
Germany
peter.pelz@fst.tu-darmstadt.de

ABSTRACT

When a fluid enters a rotating circular pipe a swirl boundary layer with thickness of $\tilde{\delta}_S$ appears at the wall and interacts with the axial momentum boundary layer with thickness of $\tilde{\delta}$. We investigate a turbulent flow applying Laser-Doppler-Anemometry to measure the circumferential velocity profile at the inlet of the rotating pipe. The measured swirl boundary layer thickness follows a power law taking Reynolds number and flow number into account. A combination of high Reynolds number, high flow number and axial position causes a transition of the swirl boundary layer development in the turbulent regime. At this combination, the swirl boundary layer thickness as well as the turbulence intensity increase and the latter yields a self-similarity. The circumferential velocity profile changes to a new presented self-similarity as well. We define the transition inlet length, where the transition appears and a stability map for the two regimes is given for the case of a fully developed axial turbulent flow enters the rotating pipe.

NOMENCLATURE

$\tilde{\square}$ Dimensional value.
A Constant in the velocity profile u_ϕ for regime II.
B Constant in the velocity profile u_ϕ for regime II.
C Constant in the growth law for δ_S.
$\tilde{R}$ Pipe radius.
$\tilde{R}_z$ Averaged surface roughness.
$Re := \frac{2\tilde{R}^2\tilde{\Omega}}{\tilde{\nu}}$ Reynolds number.
$Tu := \frac{\tilde{u}'_{\phi,\mathrm{rms}}}{(\tilde{R}\tilde{\Omega})}$ Turbulence intensity in the rotating pipe.
$Tu_z := \frac{\tilde{u}'_{\mathrm{rms}}}{\tilde{U}_{\max}}$ Turbulence intensity in the non-rotating pipe.
$\tilde{\bar{U}}$ Average axial velocity.
m_i Exponents in the growth law for δ_S.
$\tilde{r}$ Radial coordinate.
$\tilde{u}_\phi$ Circumferential velocity component.
$\tilde{y}$ Wall coordinate.
$\tilde{z}$ Axial coordinate.
Δ Measurement error.
$\tilde{\delta}$ Axial boundary layer thickness.
$\tilde{\delta}_S$ Swirl boundary layer thickness.
$\tilde{\delta}_{S07}$ Swirl boundary layer thickness with $u_\phi(\delta_{S07}, z) = 0.07$.
κ von Kármán constant.
ϕ Circumferential coordinate.
$\varphi := \frac{\tilde{\bar{U}}}{\tilde{R}\tilde{\Omega}}$ Flow number.
$\tilde{\Omega}$ Pipe angular velocity.
$\tilde{\nu}$ Kinematic viscosity.

*Address all correspondence to this author.

INTRODUCTION

At part load of a turbo machine below a critical flow number $\varphi := \tilde{\bar{U}}/(\tilde{R}\tilde{\Omega}) < \varphi_c$, with the average axial velocity $\tilde{\bar{U}}$ and circumferential velocity of the pipe $\tilde{R}\tilde{\Omega}$, flow separation occurs, the so called part load recirculation. This flow separation is caused by the swirl, i.e., centrifugal force [1, 2]. Thus, there is an interdependency of axial momentum and swirl. We use a generic model, a rotating pipe, to analyse the evolution of the swirl and the impact on axial momentum; see Fig 1. Secondary flow, e.g tip vortex, are avoided by using a rotating pipe instead of blades yielding an undisturbed flow. The outcome of this investigation is useful to analyse and to predict part load recirculation, flows in rotating gaps, e.g. secondary air flow of a gas turbine, and to clarify the inlet condition of turbo machine, e.g. a shrouded turbo machine. Thus, this investigation supports the designers of the mentioned parts of a turbo machine.

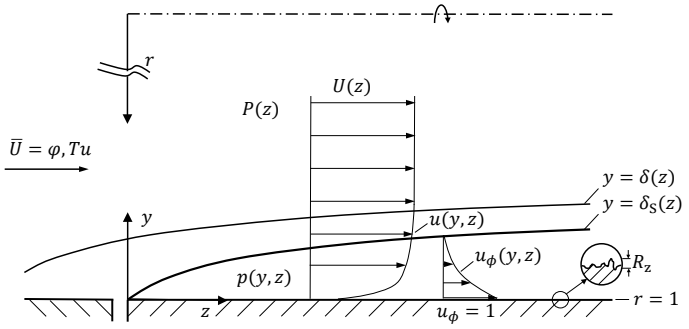

FIGURE 1. INLET OF A ROTATING PIPE.

By the generic model, an axial flow streams into the pipe and an axial boundary layer with a thickness $\tilde{\delta}$ appears and develops close to the wall. Outside the axial boundary layer, the flow is irrotational and is accelerated due to boundary layer displacement. By rotating the pipe, a second boundary layer in circumferential direction is produced by viscosity and develops. It is the so called swirl boundary layer with thickness $\tilde{\delta}_S$ [1–5]; see Fig. 1. Inside the swirl boundary layer is a circumferential velocity component $\tilde{u}_\phi$, outside, the flow is swirl-free. Due to centrifugal force, there is a non-negligible radial pressure distribution inside the swirl boundary layer for $\varphi \ll 1$ [1, 2]. The Reynolds number $Re := 2\tilde{R}^2\tilde{\Omega}/\tilde{\nu}$ with the kinematic viscosity $\tilde{\nu}$, the flow number φ and the averaged surface roughness $\tilde{R}_z$ influence the boundary layers evolution.

This paper investigates experimentally the evolution of the swirl boundary layer and the circumferential velocity profile at high Reynolds number and high flow number when a fully developed axial turbulent flow enters the rotating pipe. We observe a transition in the turbulent regime of the swirl boundary layer including a profile transformation and an increase of the turbulence intensity for a parameter combination $(Re, \varphi, z)_t$. By doing so, we measure the circumferential velocity profile by Laser-Doppler-Anemometry (LDA) and analyse the profile to indicate the turbulent regimes and the transition inlet length as it is done in our previous work [5]. Throughout this investigation, we nondimensionlise length with the pipe radius $\tilde{R}$ and velocities with the pipe circumferential velocity $\tilde{R}\tilde{\Omega}$. The superscript $\sim$ indicates dimensional values.

This paper is organized as follows: first, we give a review of the state of the art of flows in a rotating pipe. Second, the experimental set-up including measurement uncertainty is described. Third, the measurements are presented. Hereby, the circumferential velocity profile, the swirl boundary layer thickness and the turbulence intensity are the main focus. Fourth, we discuss the results concerning the the current state of the research, presented in section 2. By this discussion a stability map for the two turbulent flow regimes of the swirl boundary layer and the transition inlet length is illustrated. In the closure of this paper, we recap our investigation by six major findings.

LITERATURE REVIEW

The flow in a rotating pipe has been much more investigated at the fully developed region than at the inlet region. At the fully developed region, the boundary layers reach the pipe centre and the velocity profiles are independent of the axial coordinate. The boundary layers reach the centre for $z > 10^2$ for a turbulent flow, depending on Reynolds number and flow number [6]. Also the hydraulic losses of a turbulent flow decrease with decreasing flow number in a rotating pipe compared to a non-rotating pipe [7, 8]. The centrifugal force damps the turbulence, stronger close to the wall than in the core, and stabilizes the flow [9]. At the inlet of a rotating pipe with a turbulent flow for $\varphi > 1$, the turbulence is stimulated due to the sudden increase of the swirl for $z < 20$. Further downstream the stabilization of the centrifugal force predominates [10, 11]. The hydraulic losses are increased when a laminar flow enters a rotating pipe. For this case, the swirl destabilizes the flow, stimulates the turbulence and thus, the transition to a turbulent flow occurs further upstream than in a non-rotating pipe [8].

An interaction of the swirl and the axial momentum is observed by a complex transformation of the axial velocity profile at the inlet of a rotating pipe. Due to turbulence damping, the axial velocity profile transforms continuously from a turbulent into a laminar profile in axial direction when a fully developed, turbulent flow enters the rotating pipe [12]. This effect is called "laminarization" and has been observed in many investigations, e.g. [6, 13, 14]. The "laminarized" profile reaches the fully developed region for a small flow number. For a higher flow number, the axial velocity profile is retransformed into the turbulent one [6]. An analytical approach of this transformation

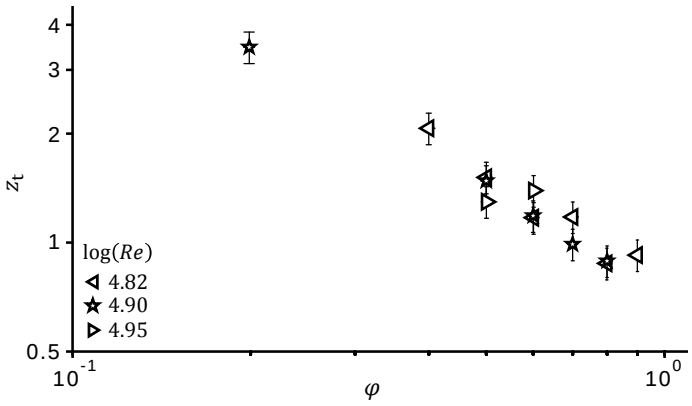

FIGURE 2. TRANSITION INLET LENGTH OF THE SWIRL BOUNDARY LAYER (CONFIGURATION I) [5].

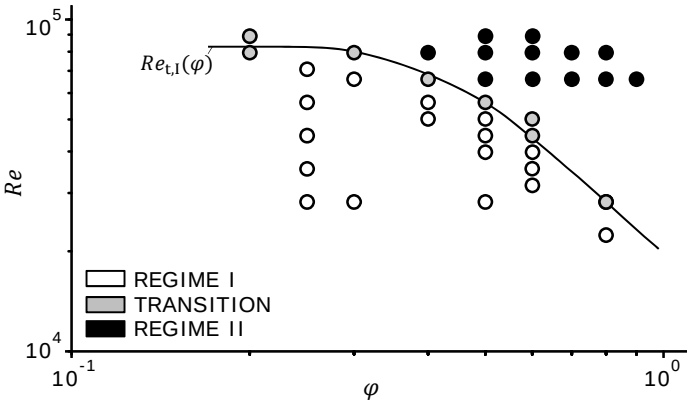

FIGURE 3. STABILITY MAP FOR REGIME I AND REGIME II OF THE SWIRL BOUNDARY LAYER (CONFIGURATION I) [5].

by Weigand and Beer [15] meets the experimental results qualitatively, but the influence of the swirl is overestimated.

The swirl boundary layer with its velocity profile defines the evolution of the swirl. The circumferential velocity profile is parabolic $u_\phi = r^2$, when a turbulent flow enters the rotating pipe [14, 16–18] and for a laminar flow it follows solid body rotation $u_\phi = r$ [14] at the fully developed region. Oberlack [19] derived the profiles by Lie group analysis. In the transition region, the circumferential velocity profile is between the parabolic and the linear profile [14]. When a thin laminar boundary layer enters a rotating pipe for $\varphi > 0.71$, the circumferential velocity profile transforms and both boundary layers are thickened at the inlet of a rotating pipe [6]. There, for a smaller flow number with a thin or fully developed turbulent or a thin laminar axial boundary layer, the circumferential velocity profile follows $u_\phi = (1-y/\delta_S)^2$ for an attached flow [1,2,4,5]. For the fully developed axial turbulent flow, the swirl boundary layer thickness follows

$$\delta_S = CRe^{m_1}\varphi^{m_2}z^{m_3}, \tag{1}$$

with $C \approx 4.43$, $m_1 \approx -0.45$, $m_2 \approx -0.46$ and $m_3 \approx 0.47$. For a thin axial boundary layer, the constant C is approximately 4.64 and $m_1 \approx -0.46$, $m_2 \approx -0.49$ and $m_3 \approx 0.44$ [2]. The swirl boundary layer becomes independent of the Reynolds number for a hydraulicly rough flow but still depends on the flow number [1, 2]. For a hydraulically rough flow, the circumferential velocity profile follows more or less $u_\phi = (1-y/\delta_S)^7$ [2].

Equation 1 for a thin axial boundary layer is confirmed by our analytical approach [1, 2]. By this approach, we use the integral method of boundary layer theory and generalize the von Kármán momentum equation taking the influence of swirl by a radial pressure distribution into account. A strong influence of the swirl on the axial momentum balance is observable for small flow numbers $\varphi \ll 1$. The swirl causes flow separation for a small flow number and a measured stability map for part load recirculation is given [1–4]. When the flow separates, the circumferential velocity profile differs from the parabolic one [1, 2, 4]. Stratford's criteria [20] is applied to derive the critical flow number for incipient separation analytically. The results are validated by experiments [1]. For small Reynolds number, e.g. laminar flow, flow separation is investigated by Lavan and others in a rotating pipe [21–23].

For high Reynolds number as well as high flow number Eqn. 1 is not longer valid because a second transition of the swirl boundary layer occurs in the turbulent regime [2, 5], which is the main focus of this paper. By this transition $(Re,\varphi,z) > (Re,\varphi,z)_t$, the circumferential velocity profile transforms from the parabolic profile $u_\phi = (1-y/\delta_S)^2$ of regime I into

$$u_\phi = -\frac{\kappa}{2}\log\left(\frac{y}{\delta_{S07}} + A\right) + B \tag{2}$$

of regime II with the von Kármán constant κ, the constants $A = 0.007$ and $B = 0.06$ and the swirl boundary layer thickness δ_{S07}, where $u_\phi(\delta_{S07}, z) = 0.07$. Furthermore, the swirl boundary layer thickens and the turbulence intensity $Tu := \tilde{u}'_{\phi,\mathrm{rms}}/(\tilde{R}\tilde{\Omega})$ increases and reaches a new self-similarity. The circumferential velocity profile transformation is applied to indicate both regimes and the transition inlet length of regime II. The transition inlet length z_t is given by Fig. 2 and indicates it is independent of the Reynolds number, thus $z_t = z_t(\varphi)$. Together with this result, the transition is described by a plane stability map $(Re,\varphi)_t$ and the transition is given by a single curve $Re_t(\varphi)$ as Fig. 3 illustrates. These findings are done when a thin axial turbulent boundary layer, i.e., configuration I, streams into the rotating pipe [5]. The transition occurs as well as when a fully developed axial turbu-

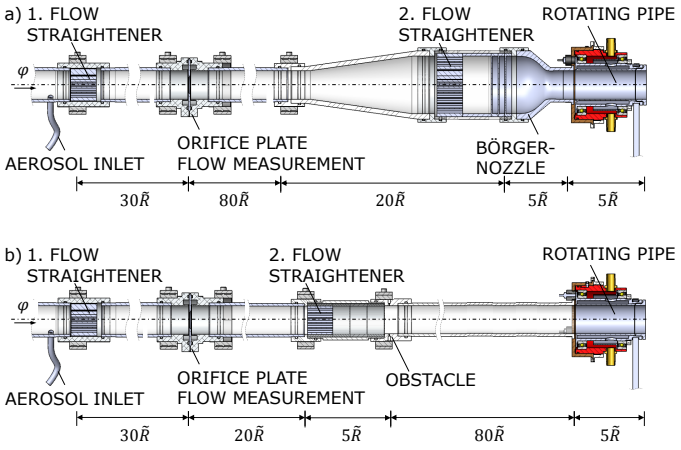

FIGURE 4. EXPERIMENTAL SET-UP WITH a) CONFIGURATION I FOR A THIN AXIAL BOUNDARY LAYER AND b) CONFIGURATION II FOR A FULLY DEVELOPED AXIAL BOUNDARY LAYER.

lent flow, i.e., configuration II, enters the rotating pipe [5], but this is not fully analysed. This is the task of this paper.

EXPERIMENTAL METHODOLOGY

A test-rig is designed to measure the evolution of the swirl boundary layer and the circumferential velocity component in a rotating pipe applying 1D LDA. The swirl boundary layer thickness depends on the Reynolds number, the flow number, the axial position and the inlet condition. By doing so, two configurations with different inlet conditions are used, cf. [1–5].

The air flow at ambient pressure is provided by a side channel blower, which increases pressure in a large plenum chamber, not shown in Fig. 4. In this plenum chamber, the air temperature is measured. The outlet of the plenum chamber is followed by a first flow straightener (cf. Fig. 4). Hence, pulsations are minimized. The volume flow is measured by an orifice plate and the flow is varied by changing the rotation speed of the blower. Thus, the axial velocity is controlled. The maximum axial velocity is 30 m/s, resulting in a Mach number smaller than 0.1.

Downstream of the flow measurement an exchangeable section for different inlet conditions is implemented; see Fig 4. Both configurations include a second flow straightener. By configuration I, three turbulence screens are installed between a diffuser and the Börger-Nozzle [24]. By means of this nozzle, a thin axial boundary layer is generated due to flow acceleration, thus a bulk like flow. Downstream of the Börger-Nozzle, the flow enters the rotating pipe as illustrated in Fig. 4. At the inlet of the rotating pipe, the axial boundary layer thickness is $\tilde{\delta}/\tilde{R} = 8\ldots10\,\%$ with a turbulent profile and $Tu_z := \tilde{u}'_{\mathrm{rms}}/\tilde{U}_{\max} \approx 1\ldots2\,\%$ outside the boundary layer for $\tilde{\tilde{U}} \geq 8\,\mathrm{m/s}$. Inside the boundary layer, the turbulence intensity increase approximately to 13 %. For configuration II, an obstacle is installed, see Fig. 4b, to generate a fully developed, turbulent boundary layer. At the inlet of the rotating pipe, the axial boundary layer thickness is 1 for $\tilde{\tilde{U}} \geq 2\,\mathrm{m/s}$. The turbulence intensity is approximately 4 % in the pipe centre and approximately 12 % closer to the wall. The inlet conditions of both configurations are measured by a hot wire anemometer.

Between the non-rotating and rotating pipe there is an axial gap of $4\,‰\tilde{R}$. The gap is sealed by sealed ball bearings. The rotating pipe radius $\tilde{R}$ is 25 mm, its length is $5\tilde{R}$ and is made of stainless steel with a relative surface roughness of $0.4\,‰\tilde{R}$. The rotating pipe is driven by a belt. The maximum rotational speed is $\tilde{\Omega} = 1308\,\mathrm{rad/s}$, yielding a maximum Reynolds number of $\log(Re) = 5.1$. Hence, Reynolds number and flow number are independent of each other. The outlet of the pipe is a free jet. The advantage of this design is a convenient accessibility from downstream to the flow field within the rotating pipe.

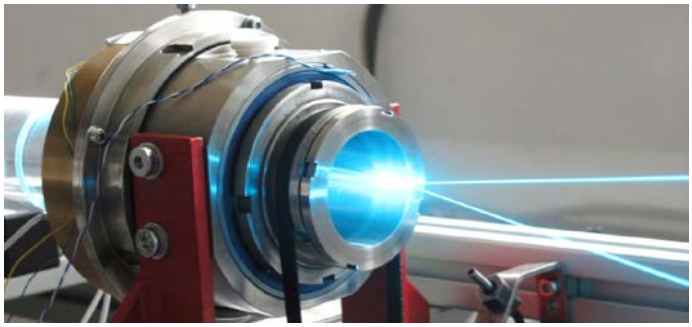

FIGURE 5. LASER BEAM PATH INTO THE ROTATING PIPE OF THE 1D LASER-DOPPLER-ANEMOMETRY.

This accessibility is used to measure only the circumferential velocity component by a 1D LDA with frequency shift and a wave length of 514.5 nm. The probe, i.e., sender and receiver, is located downstream of the rotating pipe with angle of 12° to the centreline and has a focus of 310 mm; see Fig. 5. The measurement volume has a length of $< 1.6\,\%\tilde{R}$, a diameter of $< 2\,‰\tilde{R}$ and is moveable with a two dimensional plane by using a traverse table. By doing so, the laser beams do not have to light through any solid material and are not deflected. An aerosol of silicon oil as tracer particles is added to the air to enable LDA measurements; see Fig. 4. The LDA and the experimental set-up is described in more detail by [1, 2, 4].

The measurement uncertainty are discussed in detail in previous work [2, 5]. The outcomes are the following: the Reynolds number is controlled by the rotational speed of the pipe and the air temperature. The systematic measuring error of Reynolds

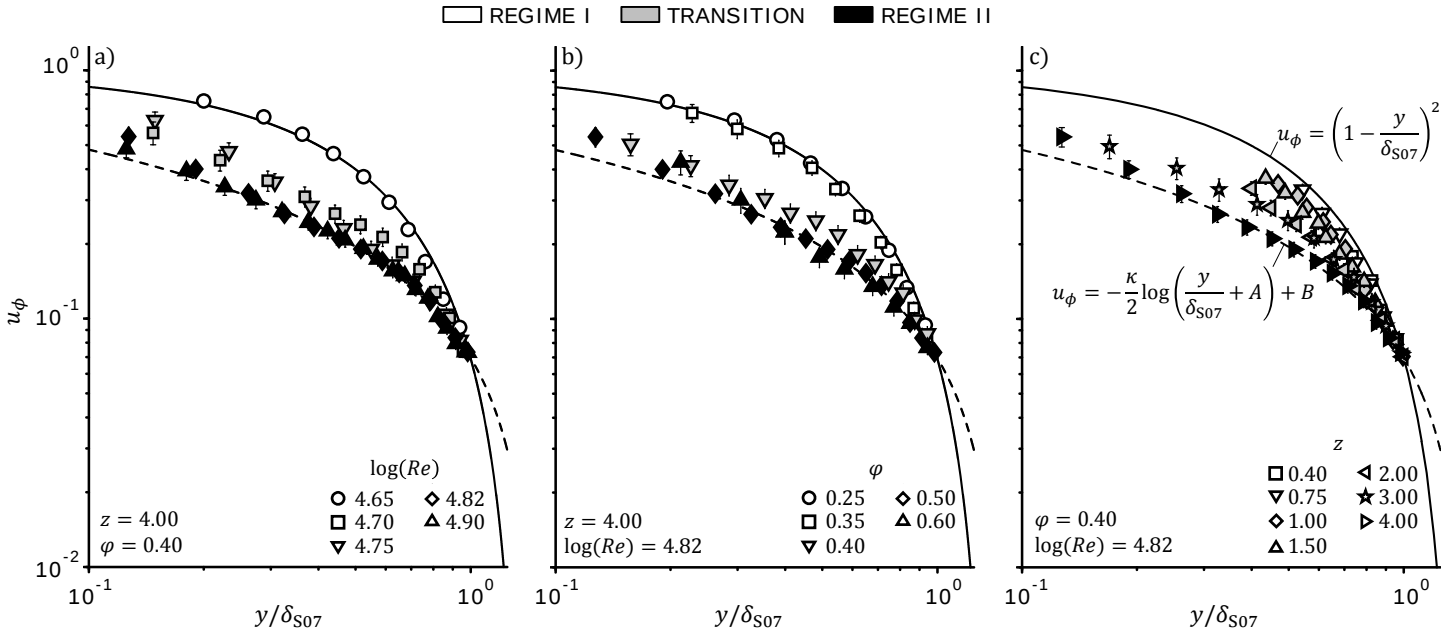

FIGURE 6. CIRCUMFERENTIAL VELOCITY PROFILE FOR a) VARIOUS REYNOLDS NUMBER, b) VARIOUS FLOW NUMBER AND c) VARIOUS AXIAL POSITION (CONFIGURATION II).

number is less than

$$\frac{\Delta Re_{\mathrm{sys}}}{Re} = \left|\frac{\Delta\tilde{\Omega}_{\mathrm{sys}}}{\tilde{\Omega}}\right| + \left|\frac{\Delta\tilde{\nu}_{\mathrm{sys}}}{\tilde{\nu}}\right| \leq \pm 4\,\% \tag{3}$$

for $\log(Re) = 4.1$. The flow number is controlled by the flow rate and is measured by an orifice plate designed in agreement with ISO 5167-2:2003 [25]. Hence, the systematic measuring error of flow number is less than

$$\frac{\Delta\varphi_{\mathrm{sys}}}{\varphi} = \left|\frac{\Delta\tilde{\Omega}_{\mathrm{sys}}}{\tilde{\Omega}}\right| + \left|\frac{\Delta\tilde{\bar{U}}_{\mathrm{sys}}}{\tilde{\bar{U}}}\right| \leq \pm 5.5\,\% \tag{4}$$

for $\varphi = 0.35$ and $\log(Re) = 4.1$. The measuring error of Reynolds number and flow number decreases with increasing Reynolds number and flow number, respectively. Both quantities are measured over 10 s including 200 data points and the 95 % confidence interval is used for the precision error.

The positioning of the LDA measuring volume has a systematic measuring error of $\Delta\tilde{z}_{\mathrm{sys}} \approx \pm 8\,‰\tilde{R}$ and $\Delta\tilde{y}_{\mathrm{sys}} \approx \pm 4\,‰\tilde{R}$. The repetitive accuracy in both directions of the traverse table is $0.8\,‰\tilde{R}$. One LDA data point is measured over more than 30 s including more than 1000 bursts. The influence of axial velocity on the measured circumferential velocity by 1D LDA is estimated by Stapp [2] and yielding $\Delta u_\phi < 10^{-2}\varphi$. The transit time of each passing tracer particle is used to weigh the measured velocity to capture the gradient diffusion error. The gradient diffusion error due to mean velocity differences across the measurement volume yields an influence of the velocity fluctuations, i.e., turbulence intensity.

In the following, all presented data points include the total measuring error by errors bars. Usually, the error bars are smaller than the marker, thus they are not visible and the precision error of $\tilde{u}'_{\phi,\mathrm{rms}}$ is unknown.

RESULTS

This section presents the measurement data gained with configuration II. By doing so, we vary Reynolds number, flow number and axial position to investigate the evolution of the swirl. First, we are presenting the circumferential velocity distribution, second, the swirl boundary layer thickness and at last the turbulence intensity $Tu := \tilde{u}'_{\phi,\mathrm{rms}}/(\tilde{R}\tilde{\Omega})$.

Circumferential Velocity Profile

Figure 6 shows the circumferential velocity profile for different Reynolds number, flow number and axial position. The velocity profile is scaled with the swirl boundary layer thickness δ_{S07}.

As it is known from our previous investigations [5], there are two turbulent regimes for the swirl boundary layer by configuration I. These two turbulent regimes are also observable by configuration II. For $(Re, \varphi, z) < (Re, \varphi, z)_{\mathrm{t}}$ the circumferential velocity

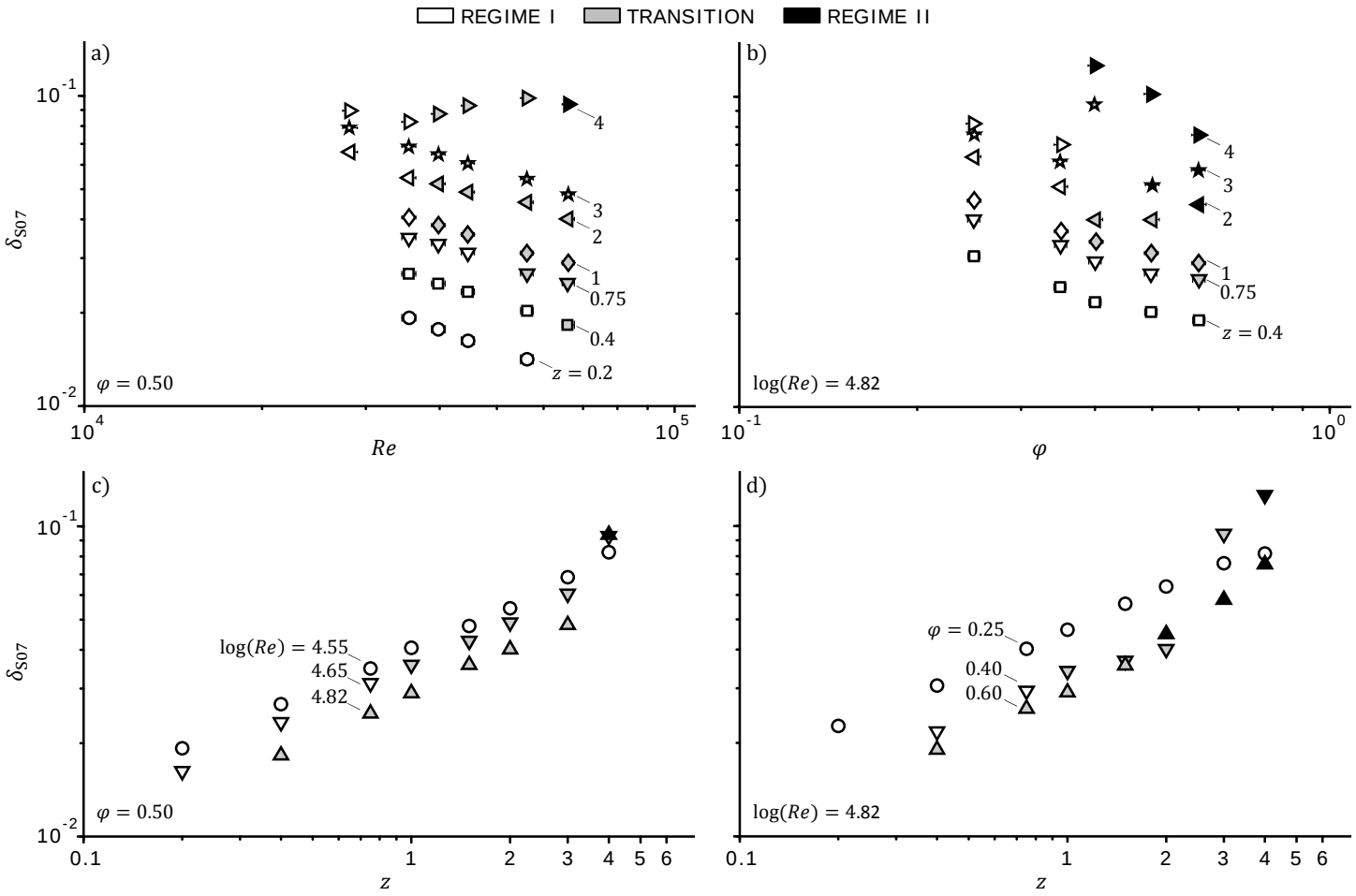

FIGURE 7. SWIRL BOUNDARY LAYER THICKNESS FOR a) AND c) CONSTANT FLOWNUMBER AND b) AND d) CONSTANT REYNOLDS NUMBER (CONFIGURATION II).

profile follows the well known parabolic profile [1,2,5,14,16–19]

$$u_\phi = \left(1 - \frac{y}{\delta_{S07}}\right)^2, \tag{5}$$

indicated by the white markers and the solid line in Fig. 6. For increasing parameters $(Re, \varphi, z) \approx (Re, \varphi, z)_t$, the circumferential velocity distribution differs from the black line, e.g. Eqn. 5. We call this the transition region which is indicated by the grey markers. Thus, there is no sharp transition surface $(Re, \varphi, z)_t$. For $(Re, \varphi, z) > (Re, \varphi, z)_t$ the circumferential velocity profile reaches a new self-similarity as it is well depictured by the black markers for regime II and the dashed line in Fig. 6. The dashed line illustrates Eqn. 2.

Swirl Boundary Layer

Figure 7 illustrates the swirl boundary layer thickness for various Reynolds number, flow number and axial position, respectively. When the swirl boundary layer reaches regime II, the swirl boundary layer thickens as the black markers in Fig. 7 show. Furthermore, the dependency of the swirl boundary layer thickness on the parameters Reynolds number, flow number and axial position changes compared with the dependency given by Eqn. 1.

Turbulence Intensity

The turbulence intensity is $2 \ldots 5\,\%$ for regime I and increases to $6 \ldots 11\,\%$ for regime II. For regime II, the turbulence intensity yields a new self-similarity as Fig. 8 shows. The self-similarity is independent of the Reynolds number, flow number and axial position, cf. Fig. 8. For the transition region, the turbulence intensity could be slightly above the new self-similarity.

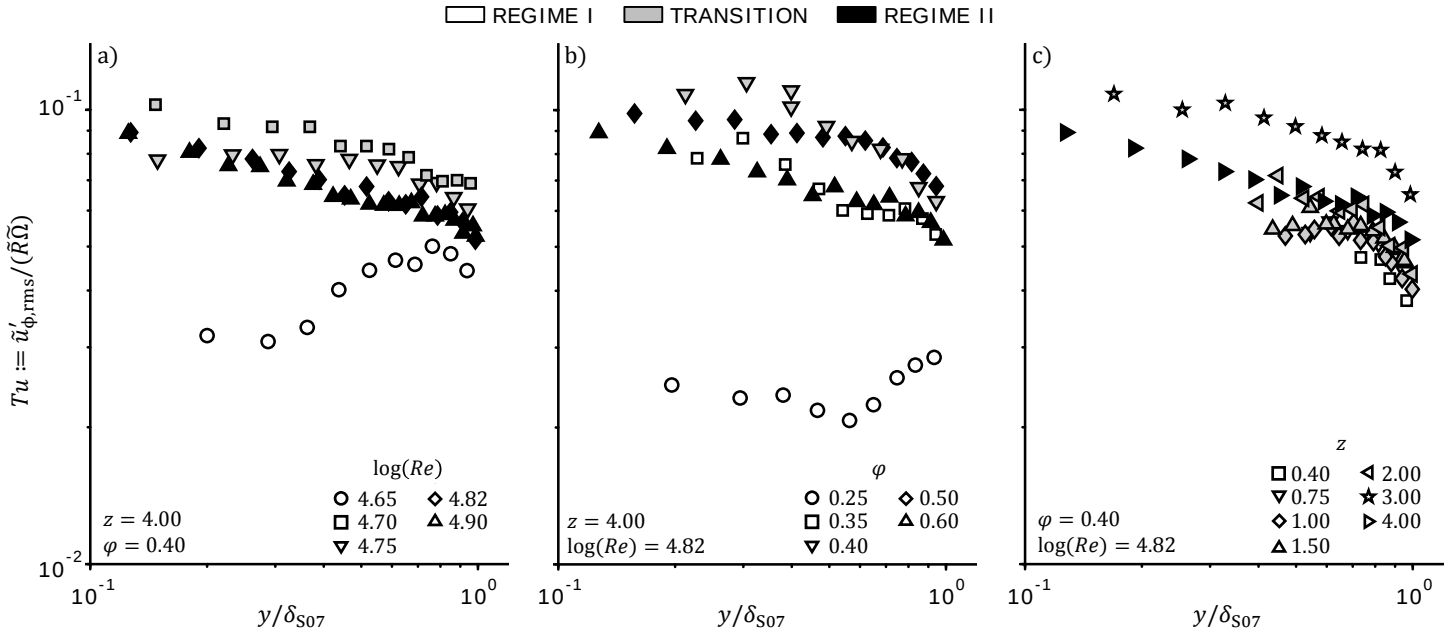

FIGURE 8. TURBULENCE INTENSITY FOR a) VARIOUS REYNOLDS NUMBER, b) VARIOUS FLOW NUMBER AND c) VARIOUS AXIAL POSITION (CONFIGURATION II).

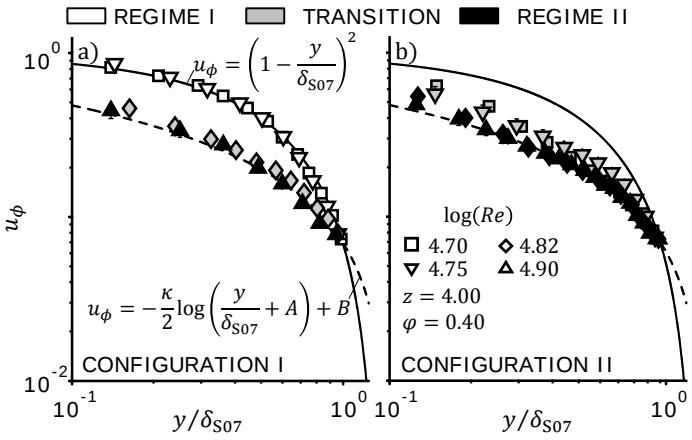

FIGURE 9. COMPARE OF CIRCUMFERENTIAL VELOCITY PROFILE BY VARIOUS REYNOLDS NUMBER FOR a) CONFIGURATION I AND b) CONFIGURATION II.

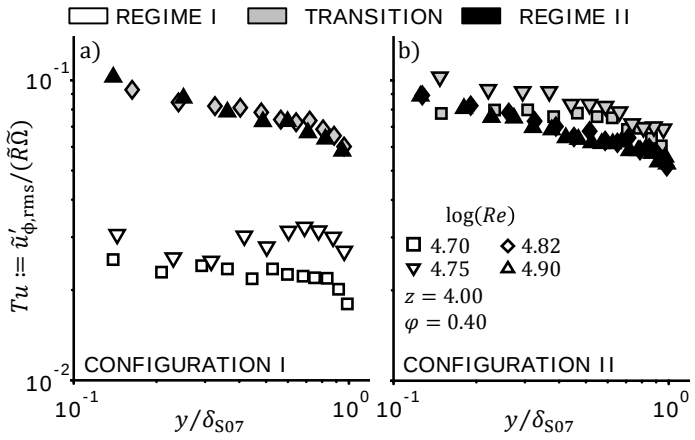

FIGURE 10. COMPARE OF TURBULENCE INTENSITY BY VARIOUS REYNOLDS NUMBER FOR a) CONFIGURATION I AND b) CONFIGURATION II.

DISCUSSION

As it is discussed by our paper when a thin axial turbulent boundary layer enters the rotating pipe [5], regime II is neither the hydraulically rough state nor a flow separation although the circumferential velocity profile and the turbulence intensity are similar to these cases. The swirl boundary layer thickness still depends on the Reynolds number. This is not the case for the hydraulically rough state [1, 2]. The critical flow number for flow separation is $\varphi_c = 0.1 \ldots 0.2$ as our previous investigations indicates [1–4]. Here, we are well above this critical range.

Facciolo et al. [26] presented a calculation of the circumferential velocity profile at the fully developed region with the angular momentum balance and shows, that the Reynolds stress $\overline{u'u'_\phi}$ transforms this profile from the linear to the parabolic profile. An increase of the turbulence intensity could justify the profile transformation at the developing inlet region. Thus, our findings indicate an up to now unknown transition to a second turbulent regime when a fully developed axial turbulent flow streams in a

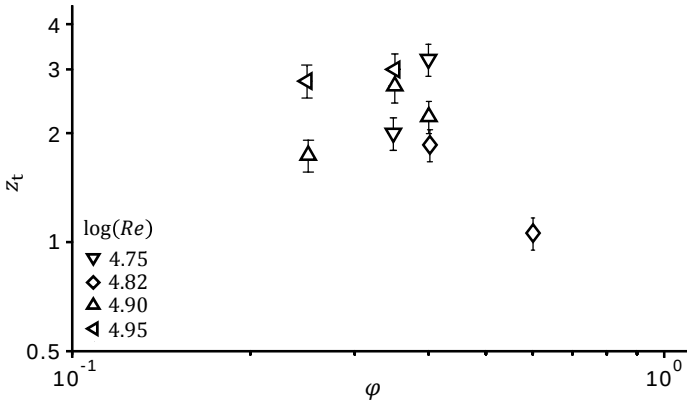

FIGURE 11. TRANSITION INLET LENGTH OF THE SWIRL BOUNDARY LAYER (CONFIGURATION II).

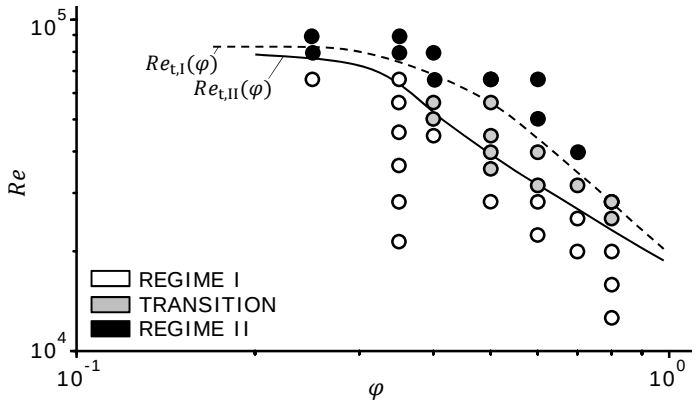

FIGURE 12. STABILITY MAP FOR REGIME I AND REGIME II OF THE SWIRL BOUNDARY LAYER (CONFIGURATION II). THE SOLID LINE INDICATES THE TRANSITION REGION FOR CONFIGURATION II AND THE DASHED LINE FOR CONFIGURATION I FROM FIG. 3.

rotating pipe.

Now, we are discussing the influence of the incoming flow, e.g. configuration I vs. configuration II. Hereby, the circumferential velocity profile and the turbulence intensity are analysed. Figure 9 illustrates the circumferential velocity profile for both configuration at various Reynolds number with two major findings: first, independent of the incoming flow, the circumferential velocity profile transforms according to Eqn. 2 by regime II. Thus, the circumferential velocity profile for regime II is independent of the incoming flow, e.g. configuration I or II. Second, for configuration II the transition to regime II begins for smaller Reynolds number as for configuration I.

Figure 10 shows the turbulence intensity for the same parameter combination and set-up as Fig. 9 does. Independent of configuration I or II, the turbulence intensity yields the same self-similarity. By the transition of the swirl boundary layer, the turbulence intensity is slightly increased for configuration II compared to configuration I. The second finding by the circumferential velocity profile analysis is confirmed by Fig. 10.

We apply our self-developed method to indicate the transition [5]. The two circumferential velocity profiles, Eqn. 5 for regime I and Eqn. 2 for regime II, are used to indicate the flow regime. By doing so, we identify the transition inlet length for configuration II; see Fig. 11. For configuration I, it seems that the transition inlet length z_t is independent of the Reynolds number; cf. Fig. 2 and [5]. The investigation of this paper with configuration II could not confirm this independence. The transition inlet depends on the Reynolds number and is between $1.5 \leq z_t \leq 3$. At the very end, it could be that the method to indicate the regimes and therefore the transition inlet length needs to be improve to clarify the dependency of the transition inlet length on the Reynolds number for configuration II. Furthermore, instead of a sharp transition point as Fig. 11 illustrates a transition area might be possible for configuration II in contrast to the results for configuration I; cf. [5].

A stability map for configuration II, whether regime I or regime II occurs, is given by Fig. 12. The solid line indicates the transition region $Re(\varphi)_{t,II}$ for configuration II and the dashed line $Re(\varphi)_{t,I}$ for configuration I. Our previous findings in this section are confirmed, that the transition begins by smaller parameter combination for configuration II as by configuration I $(Re,\varphi,z)_{t,I} > (Re,\varphi,z)_{t,II}$. For smaller flow number, the transition lines $Re(\varphi)_{t,I}$ and $Re(\varphi)_{t,II}$ seem to be similar.

CONCLUSION

This paper analysed the evolution of swirl at high Reynolds number and high flow number at the inlet of a rotating pipe with a length of $5\tilde{R}$. The incoming flow is a fully developed axial turbulent flow, i.e., configuration II. The swirl distribution and evolution follows the known regularity for $(Re,\varphi,z) < (Re,\varphi,z)_t$, regime I. For $(Re,\varphi,z) > (Re,\varphi,z)_t$, we observed a second transition in the turbulent regime as we did in our previous work for a thin axial turbulent flow enters the rotating pipe [5], i.e., configuration I. Recapping this paper, we have six major findings:

1. The transition from regime I into regime II is observable for both configurations.
2. For regime II, the circumferential velocity profile follows $u_\phi = -\frac{\kappa}{2}\log\left(\frac{y}{\delta_{S07}}+0.007\right)+0.06$ for both configurations.
3. The swirl boundary layer thickens for regime II and changes the dependency on Reynolds number, flow number and axial position for both configurations.
4. The turbulence intensity increases for regime II and yields a new self-similarity independent of the configurations.
5. Whether and where regime II for configuration II appears is given by the transition inlet length, cf. Fig. 11 and the

stability map Fig. 12. The transition inlet length depends on the Reynolds number for configuration II in contrast to the results for configuration I.

6. The transition begins by higher parameter combination for configuration I as for configuration II $(Re, \varphi, z)_{\mathrm{t,I}} > (Re, \varphi, z)_{\mathrm{t,II}}$; cf. Fig. 12.

The results and findings of the presented work may serve to predict the incoming flow of a turbo machine, e.g. a shrouded turbo machine and flow in rotational gaps, e.g. secondary air flow of a gas turbine. Therefore, secondary flow due to incidence and part load recirculation could be avoided considering the second turbulent regime and the previous investigations [1–5] for designing a turbo machine or rotating gaps.

The investigation of the axial boundary layer is necessary to analyse the transition completely. Thus, the axial boundary layer is in the next research focus.

ACKNOWLEDGMENT

The authors would like to thank the German Research Foundation DFG for funding this research within PE 1573/5-1.

References

[1] Cloos, F.-J., Stapp, D., and Pelz, P., 2015. Swirl boundary layer and flow separation at the inlet of a rotating pipe. Submitted to J. Fluid Mech.

[2] Stapp, D., 2015. *Experimentelle und analytische Untersuchung zur Drallgrenzschicht*. Forschungsberichte zur Fluidsystemtechnik, Technische Universität Darmstadt.

[3] Stapp, D., Pelz, P., and Loens, J., 2013. "On part load recirculation of pumps and fans - a generic study". In Proceedings of the 6th International Conference On Pumps an Fans with Compressors and Wind Turbines, p. 022003.

[4] Stapp, D., and Pelz, P., 2014. "Evolution of swirl boundary layer and wall stall at part load - a generic experiment". In Proceedings of ASME Turbo Expo GT2014–26235.

[5] Cloos, F.-J., Zimmermann, A.-L., and Pelz, P., 2016. Two turbulent flow regimes at the inlet of a rotating pipe. Accepted to 16 International Symposium on Transport Phenomena and Dynamics of Rotating Machinery.

[6] Nishibori, K., Kikuyama, K., and Murakami, M., 1987. "Laminarization of turbulent flow in the inlet region of an axially rotating pipe". *Bulletin of JSME,* ***30***, pp. 255–262.

[7] Levy, F., 1927. "Strömungserscheinungen in rotierenden Rohren". PhD thesis, Technischen Hochschule München.

[8] White, A., 1964. "Flow of a fluid in an axially rotating pipe". *J. Mech. Engng. Sc.,* ***6***, pp. 47–52.

[9] Borisenko, A., Kostikov, O., and Chumachenko, V., 1973. "Experimental study of turbulent flow in a rotating channel". *J. Engng. Phys. and Thermophys,* ***24***, pp. 770–773.

[10] Nagib, H., Lavan, Z., Fejer, A., and Wolf, L., 1973. "Experimental study of turbulent flow in a rotating channel". *J. Engng. Fluids,* ***24***, pp. 770–773.

[11] Bissonnette, L., and Mellor, G., 1974. "Experiments on the behavior of an axisymmetric turbulent boundary layer with a sudden circumferential strain". *J. Fluid Mech.,* ***63***, pp. 369–413.

[12] Kikuyama, K., Murakami, M., Nishibori, K., and Maeda, K., 1983. "Flow in an axially rotating pipe. a calculation of flow in the saturated region". *Bulletin of JSME,* ***26***, pp. 506–513.

[13] Weigand, B., and Beer, H., 1994. "On the universaility of the velocity profiles of a turbulent flow in an axially rotating pipe". *Appl. Sc. Research,* ***52***, pp. 115–132.

[14] Imao, S., Itohi, M., and Harada, T., 1996. "Turbulent characteristics of the flow in an axially rotating pipe". *Int. J. of heat and fluid flow,* ***17***(5), pp. 444–451.

[15] Weigand, B., and Beer, H., 1992. "Fluid flow and heat transfer in an axially rotating pipe: the rotational entrance". In Proceedings of the 3rd ISROMAC, pp. 325–340.

[16] Murakami, M., and Kikuyama, K., 1980. "Turbulent flow in axially rotating pipes". *J. Fluids Engng.,* ***102***, pp. 97–103.

[17] Kikuyama, K., Murakami, M., and Nishibori, K., 1983. "Developement of three-dimensional turbulent boundary layer in an axially rotating pipe". *J. Fluids Engng.,* ***105***, pp. 154–160.

[18] Reich, G., 1988. "Strömung und Wärmeübertragung in einem axial rotierenden Rohr". PhD thesis, Technischen Hochschule Darmstadt.

[19] Oberlack, M., 1999. "Similarity in non-rotating and rotating turbulent pipe flows". *J. Fluid Mech.,* ***379***, pp. 1–22.

[20] Stratford, B., 1959. "The prediction of separation of the turbulent boundary layer". *J. Fluid Mech.,* ***5***, pp. 1–16.

[21] Lavan, Z., Nielsen, H., and Fejer, A., 1969. "Separation and flow reversal in swirling flows in circular ducts". *Phys. Fluids,* ***12***, pp. 1747–1757.

[22] Imao, S., Zhang, Q., and Yamada, Y., 1989. "The laminar flow in the developing region of a rotating pipe". *Bulletin of JSME,* ***32***, pp. 317–323.

[23] Crane, C., and Burley, D., 1976. "Numerical studies of laminar flow in ducts and pipes". *J. Comp. and appl. Mathe.,* ***2***, pp. 95–111.

[24] Börger, G.-G., 1973. "Optimierung von Windkanaldüsen für den Unterschallbereich". PhD thesis, Ruhr-Universität Bochum.

[25] ISO 5167-2:2003 Measurement of fluid flow by means of pressure differential devices inserted in circular cross-section conduits running full - Part 2: Orifice plates.

[26] Facciolo, L., Tillmark, N., Talamelli, A., and Alfredsson, P., 2007. "A study of swirling turbulent pipe and jet flows". *Phys. Fluids,* ***19***, pp. 1–18.